

The solar neutrino problem after three hundred days of data at SuperKamiokande

G. L. Fogli, E. Lisi, and D. Montanino
Dipartimento di Fisica and Sezione INFN di Bari,
Via Amendola 173, I-70126 Bari, Italy

Abstract

We present an updated analysis of the solar neutrino problem in terms of both Mikheyev-Smirnov-Wolfenstein (MSW) and vacuum neutrino oscillations, with the inclusion of the preliminary data collected by the SuperKamiokande experiment during 306.3 days of operation. In particular, the observed energy spectrum of the recoil electrons from ^8B neutrino scattering is discussed in detail and is used to constrain the mass-mixing parameter space. It is shown that: 1) the small mixing MSW solution is preferred over the large mixing one; 2) the vacuum oscillation solutions are strongly constrained by the energy spectrum measurement; and 3) the detection of a possible semi-annual modulation of the ^8B flux due to vacuum oscillations should require at least one more year of operation of SuperKamiokande.

PACS number(s): 26.65.+t, 13.15.+g, 14.60.Pq

I. INTRODUCTION

The solar neutrino problem [1], namely, the deficit of the neutrino rates measured by the four pioneering solar neutrino experiments, Homestake [2], Kamiokande [3], SAGE [4], and GALLEX [5], as compared to the standard solar model predictions [6], represents one of the most convincing indications for new physics beyond the standard electroweak theory. On the one hand, the confidence in the performances of the four detectors has increased continuously, as a result of many careful experimental cross-checks and calibrations [7-10]. On the other hand, the reliability of the most refined solar evolution models (including light element diffusion) has been corroborated by the impressive agreement with a growing amount of helioseismological data [11,12]. Therefore, new neutrino physics (such as neutrino oscillations) appears to be a likely solution of the solar deficit.

However, the deficit of the neutrino event rate is a solar model dependent quantity. It is highly desirable, instead, to measure observables whose interpretation is not related to a prior knowledge of the absolute neutrino flux, such as shape deviations of energy spectra, or relative variations of the event rates during the time of the year. Such measurements have been pioneered by the Kamiokande experiment [8], but with statistics too low to provide definitive indications. This experimental program is now being pursued with much higher statistics by the real-time, water-Cherenkov SuperKamiokande experiment [13].

The preliminary results after the first 306.3 days of operation of SuperKamiokande [14-16] are already sufficiently accurate to provide interesting new insights into the solar neutrino problem, although further data are required to draw decisive conclusions. Therefore, we think it useful to present an updated analysis of the solar neutrino problem, including the most recent results from the four pioneering experiments [17,18,19] and from the SuperKamiokande experiment after 306.3 days [14-16], that have become publicly available during the 1997 summer conferences. In particular, we discuss in detail the information provided by the energy spectrum of recoil electrons observed at SuperKamiokande, which is one of the most important solar model independent observables. The available experimental information is interpreted in the light of two-flavor neutrino oscillations, both in vacuum [20] and in matter, according to the Mikheyev-Smirnov-Wolfenstein (MSW) mechanism [21].

The paper is organized as follows. In Sec. II we analyze the solar neutrino problem using the available solar model dependent information (namely, the absolute neutrino rates). In Sec. III we analyze the solar model independent information, and in particular the electron energy spectrum measured by SuperKamiokande, in order to constrain the oscillation interpretation both in matter and in vacuum. We draw our conclusions in Sec. IV. Some technical aspects of the energy spectrum analysis are elucidated in the Appendix.

II. SOLAR MODEL DEPENDENT INFORMATION

In this section we report the most recent measurements of the solar neutrino rates, and compare them to the expectations of the 1995 Bahcall-Pinsonneault (BP95) standard solar model [6]. The observed deficit is interpreted in terms of MSW and vacuum two-family oscillations in the parameter space spanned by the neutrino squared mass difference Δm^2 and by the mixing angle θ .

A . The solar neutrino deficit

Table I reports the neutrino event rates measured by the four pioneering solar neutrino experiments Homestake [17], Kamikande [8], SAGE [18], and GALLEX [19], together with the ^8B neutrino flux measurement after 306.3 days at SuperKamikande [14{16]. The observed rates appear to be significantly smaller than the theoretical expectations of the BP95 model.

Figure 1 shows graphically the information reported in Table I, with the further inclusion of the correlations of theoretical uncertainties, which have been calculated as in [22]. In Fig. 1 the GALLEX and SAGE data have been combined (in quadrature) in a single (Gallium) result. The same has been done for the Kamikande and SuperKamikande data (K + SuperK). In the combination, asymmetric errors have been conservatively symmetrized to the largest one. The 99% C.L. experimental and theoretical ellipses appear to be distinctly separated in all the planes charted by any two experiments. Notice that the (strongly correlated) theoretical errors are rather large as compared to the experimental errors. Therefore, as far as the total neutrino rates are concerned, further reductions of the experimental uncertainties are not expected to change significantly the current picture of the solar deficit, while improvements in the theoretical predictions would have a greater impact.

B . MSW and vacuum oscillations

As is well known, a viable explanation of the solar neutrino deficit is represented by matter-enhanced (MSW) neutrino oscillations (see, e.g., [23{25]) or, alternatively, by vacuum neutrino oscillations (see, e.g., [26,25]). Assuming for simplicity oscillations between two families, the analysis involves only two parameters, the neutrino squared mass difference m^2 and the mixing angle θ .

Figure 2 shows the results of our χ^2 -analysis of the data reported in Table I, assuming MSW oscillations. Notice that this fit includes only the deficit data, and not the solar model independent information provided by the energy spectra or the night-day asymmetry (that will be considered separately in Sec. III). The usual small and large mixing angle solutions appear to be slightly more constrained than in previous fits (see, e.g., [24]), mainly as a result of the new SuperKamikande data. The absolute minimum of χ^2 ($\chi^2_{\text{min}} = 1.0$) is reached at $(m^2; \sin^2 2\theta) = (9.6 \cdot 10^{-6} \text{ eV}^2; 4.8 \cdot 10^{-3})$; the secondary minimum ($\chi^2_{\text{sec}} = 2.45$) is reached at $(m^2; \sin^2 2\theta) = (1.5 \cdot 10^{-5} \text{ eV}^2; 0.58)$. The 90, 95, and 99% C.L. allowed regions coincide with the contours at $\chi^2 - \chi^2_{\text{min}} = 4.61, 5.99$, and 9.21, respectively.

Figure 3 shows the analogous results for the vacuum oscillation analysis. We find the minimum value $\chi^2_{\text{min}} = 4.0$ at $(m^2; \sin^2 2\theta) = (8.2 \cdot 10^{-11} \text{ eV}^2; 0.87)$. A comparison of χ^2_{min} seems to indicate a preference of the MSW oscillation scenario over the vacuum oscillation one. However, it should be noted that, in vacuum oscillation fits, the value of χ^2_{min} is very sensitive to small shifts in the central values of the experimental results and thus it might change significantly with new data (while it turns out to be more stable in MSW fits).

A few technical remarks are in order. In our oscillation analyses, the GALLEX and SAGE data have been combined in quadrature. However, the Kamikande and SuperKamikande data have been fitted separately, since these two experiments have different thresholds and

energy resolutions. In particular, according to [16], we use for SuperKamioke a threshold of 6.5 MeV for the total electron energy E_e , and a Gaussian energy resolution function with a full width of 15% at $T = 10 \text{ MeV}$ ($T = E_e - m_e$), scaling as $1/\sqrt{T}$ at different electron kinetic energies. The input neutrino fluxes have been taken from [6], and the corresponding theoretical uncertainties have been included in the 2×2 covariance matrix as in [22]. Asymmetric errors have been conservatively symmetrized to the largest one. The ^8B neutrino energy spectrum has been taken from [27].¹ Concerning the neutrino cross sections, we use the updated calculations of [27] for the chlorine experiment, and of [28] for the water-Cherenkov experiments. In the MSW calculations, the neutrino production regions and the electron density profiles have been taken from [6]. The Earth regeneration effect is included analytically as in [29] for each detector latitude. In the vacuum oscillation calculations, the time average over the year is performed through the analytical approach of [30]. In conclusion, Figs. 2 and 3 represent state-of-the-art results in the field of solar neutrino oscillations.

III. SOLAR MODEL INDEPENDENT INFORMATION

In this section we analyze the solar model independent information about the electron energy spectrum and the time variation of the neutrino rate measured by SuperKamioke. Since these data are already more accurate than the corresponding Kamioke ones, we do not include the latter in our analysis.

We recall that the SuperKamioke experiment has collected a total of 4395 solar neutrino events above threshold ($E_e > 6.5 \text{ MeV}$) during 306.3 days of operation with a fiducial volume of 22.5 kton [14{16], corresponding to an observed rate of 0.6377 events/day/kton. Given the quoted detection factor of 0.3685 [14] (see also Table I), the expected rate (BP95 model, no oscillation) is equal to 1.730 events/day/kton.

A. Energy spectrum

The SuperKamioke experiment has measured the energy spectrum of recoil electrons from ν -e scattering. The spectrum is given [14{16] in the form of a 16-bin histogram, each bin presenting the ratio between the experimental rate and the theoretical rate. Since the theoretical spectrum has not been explicitly presented, we rely upon our calculations, using for SuperKamioke the same inputs (^8B spectrum, cross section, energy resolution and threshold) described in the previous section, and normalizing the results to the total expected rate of 1.730 events/day/kton. The global information about the energy spectrum is reported in Table II and in Fig. 4.

¹The ^8B spectrum shape errors evaluated in [27] have not been included in the fits of Figs. 2 and 3, since their effect is much smaller than the uncertainty in the absolute ^8B neutrino flux. However, such shape errors will be included in the analysis of the energy spectrum performed in Sec. III and in the Appendix.

Table II shows the relevant spectral data in each of the 16 bins (numbered in the first column). As shown in the second column, all bins have a 0.5 MeV width, with the exception of the last one, which collects all events between 14 and 20 MeV (total energy). The third and fourth column report the average total energy E_i (in MeV) and the expected event rate n_i (in events/day/kton/bin) for each bin, in the absence of oscillations (our calculation). The sum of the entries in the fourth column gives the expected rate of 1.730 events/day/kton. The fifth column reports the ratio r_i between the experimental and theoretical rate in each bin. The upper and lower errors of r_i are given in the following columns. The sixth and seventh columns report the quadratic sum of statistical and uncorrelated systematic errors (σ_i^0). Finally, the correlated systematic errors (σ_i^0) are given in the last two columns. The data in columns 6-9 have been graphically reduced from the plots shown in [14-16] and thus may be subject to slight inaccuracies. The numbers are given with three decimal places just to avoid further errors due to truncation and round-off. The asymmetry between upper and lower errors is mainly due to two slightly different energy calibration procedures [16]. Shifts in the absolute energy scale represent the most important source of systematic uncertainties, as was emphasized earlier in [31,32].

Figure 4 shows the spectral information in a different way. The solid curve represents our calculation of the electron spectrum, using the best-fit ^8B neutrino spectrum given in [27]. The shape of the ^8B neutrino spectrum is subject to some uncertainties, that have been carefully evaluated in [27]. Therefore, we have also used the ± 3 deviated neutrino spectra reported in [27] to calculate the effect on the electron spectrum (dotted curves). Notice that in Fig. 4 both the central and the ± 3 deviated theoretical electron spectra are renormalized to the same total area as the experimental spectrum (0.6377 events/day/kton). The black circles represent the experimental spectrum, with horizontal error bars spanning the bin widths, and vertical error bars representing the 1σ total experimental uncertainties (quadratic sum of statistical and systematic errors). It can be seen that the slope of the experimental spectrum is slightly more gentle than the theoretical spectrum, the rate observed at low (high) energies being somewhat suppressed (enhanced) with respect to the expectations. This indication, if combined with significantly smaller errors, would represent unmistakable evidence for a new, energy-dependent process (such as flavor oscillations) affecting solar neutrinos along their path to the Earth.

Since the observed spectrum deviates only slightly from the expected one, it is reasonable to try to "summarize" the spectral information in a single parameter, related in some way to the slope deviation. We adopt the approach advocated in Refs. [31,32,29], where the spectral deformations were expanded in a series of deviations of the spectral moments (the mean, the variance, etc.) from their standard values. Given the present experimental uncertainties, it is sufficient to study the deviations of the first moment, namely, of the average kinetic energy $\langle T \rangle$ of the electrons, from its standard (no oscillation) value $\langle T \rangle_0$. This reduction procedure has the practical advantage that a single parameter ($\langle T \rangle$) is used in the fits, instead of 16 bins with correlated errors.

Since the value of $\langle T \rangle$ has not been reported in [14-16], we have estimated it from the energy spectrum information presented in Table II and in Fig. 4. The reader is referred to the Appendix for a detailed derivation. Our result for the fractional deviation $\langle T \rangle = \langle T \rangle_0 (1 + \delta)$ is:

$$\frac{hT i - hT i_0}{hT i_0} \cdot 100 = 0.99^{+2.52}_{-0.96} ; \quad (1)$$

where the errors represent the total uncertainties at 1 σ . This result represents the starting point of our analysis of the energy spectra deviations due to oscillations. It can be noticed that the observed value of $hT i$ is about 1% higher than the expectations, with an upper error larger than the lower one. Therefore, negative deviations of $hT i$ (i.e., negative "tilts" of the spectrum slope) will be much more constrained than positive deviations.

B. Time variations

Possible variations of the neutrino rate during the night would represent evidence for the a regeneration of ν_e 's in the Earth matter, as expected within the MSW scenario (see, e.g., [29] and references therein). The SuperKamioKANDE experiment has found no such effect within the present uncertainties. In fact, the measured asymmetry between nighttime (N) and daytime (D) neutrino rates is [14]{16]

$$\frac{N - D}{N + D} = 0.017 \pm 0.026 \text{ (stat.)} \pm 0.017 \text{ (syst.)} ; \quad (2)$$

No evidence for variations of the neutrino rate during the time of the year has been found so far [14]. Semiannual modulations of the signal (in addition to the trivial $1=L^2$ geometrical variations) would indicate the presence of neutrino oscillations in vacuum (see, e.g., [30,33] and references therein). A Fourier analysis of the signal expected in SuperKamioKANDE shows that this experiment is sensitive only to the first harmonic f_1 which, in the absence of oscillations, is equal in value to the Earth's orbit eccentricity $e = 0.0167$ (see [33] for details). The purely statistical error σ_f of the difference $f_1 - e$ is given by [33]

$$\sigma_f = \sqrt{\frac{N_S + N_B}{2N_S^2}} ; \quad (3)$$

where N_S and N_B are the number of signal and background events, respectively.

The numbers N_S and N_B depend on the cut applied to the declination angle in the direction of the sun (δ_{sun}). Using Eq. (3) and the spectrum of $N_S + N_B$ in terms of $\cos \delta_{\text{sun}}$ as reported in [14]{16], we derive the values of σ_f shown in Table III. The dependence of σ_f on the cuts applied to $\cos \delta_{\text{sun}}$ turns out to be weak, since the effect of a lower signal tends to be compensated by a better signal-to-background ratio, and vice versa. On the basis of the results reported in Table III, we assume

$$\sigma_f = 0.020 \text{ (1 yr)} \quad (4)$$

as the typical statistical error of the first Fourier harmonic, after one year of operation at SuperKamioKANDE. The errors corresponding to 2 and 4 years of operation are simply obtained with rescaling factors of $1/\sqrt{2}$ and $1/2$, respectively (assuming the current background event rate). Possible systematic errors that might affect the determination of f_1 are not considered here.

C . Im plications for oscillations in m atter

Figure 5 illustrates the im plications of the electron energy spectrum m easured by SuperK am iokande [as sum m arized by the datum of Eq. (1)] for the M SW scenario. The upper panel shows curves at constant values of the fractional deviation of $h\Gamma i$ expected in the presence of M SW oscillations. Sim ilar curves were discussed earlier in [29] (w ith a di erent energy threshold) and in [32] (w ithout the Earth regeneration e ect). Superposed are the sm all and large m ixing angle solutions found in Fig. 2 (at 95% C.L.). The central value in Eq. (1) is intriguingly close to the values of $h\Gamma i = h\Gamma i_0$ w ithin the sm all m ixing angle solution, w hich thus appears slightly favored as com pared to the large m ixing one. Unfortunately, the errors in Eq. (1) are still large, so that only excluded regions can be m eaningfully derived at present. The lower panel shows the regions excluded at 2, 3, and 4 standard deviations by Eq. (1). For instance, in the regions excluded at the 2 level, the theoretical value of $h\Gamma i = h\Gamma i_0$ is either sm aller than -0.93% or greater than $+6.05\%$. The excluded regions are sim ilar to those shown by the SuperK am iokande Collaboration [14{16].

Figure 6 illustrates the im plications of the night-day asym m etry datum of Eq. 2 for the M SW scenario. The upper panel shows iso-lines of the night-day asym m etry (percentage) expected in the presence of oscillations. The lower panel shows the regions excluded at 2, 3 and 4 standard deviations by the datum of Eq. 2. The lower part of the large angle solution, w here the asym m etry is predicted to be $\sim 10\%$, appears to be disfavored by the experim ental results.

W e do not attempt here a global χ^2 -com bination of all the SuperK am iokande data (total rate, energy spectrum , and night-day variations), since these pieces of inform ation are not independent; in fact, they are just di erent "projections" of the double di erential spectrum of events as a function of tim e and energy. A proper analysis of the w hole SuperK am iokande data w ill be possible w hen such spectrum and its uncertainties w ill become available.

In conclusion, the present data seem to favor the sm all angle solution w ith respect to the large m ixing one, because: 1) The global value of χ^2 is lower at the sm all m ixing solution; 2) The energy spectrum shows a slight deviation consistent w ith sm all m ixing; 3) Part of the large m ixing angle solution is disfavored by the nonobservation of a large night-day asym m etry.

D . Im plications for oscillations in vacuum

Figure 7 illustrates the im plications the energy spectrum m easurement [as sum m arized by the datum in Eq. (1)] for the vacuum oscillation scenario. The upper panel shows curves at constant values of the fractional deviation of $h\Gamma i$ expected in the presence of vacuum oscillations. Sim ilar curves were discussed earlier in [32] (w ith a di erent energy threshold for SuperK am iokande). Superposed are the m ulti ple solutions found in the vacuum oscillation t of Fig. 3 (at 95% C.L.). The solutions at "low m^2 " ($m^2 < 6\{7.5 \cdot 10^{11} \text{ eV}^2$) predict positive deviations of $h\Gamma i$, in agreem ent w ith the datum of Eq. (1). The "high m^2 " solutions predict negative deviations, and thus are strongly disfavored, as shown in the lower panel of Fig. 7. Sim ilar results have been discussed by the SuperK am iokande Collaboration [14{16], and are consistent w ith earlier K am iokande spectrum ts [25].

Figure 8 illustrates the sensitivity of the SuperKamioke experiment to semiannual modulations of the neutrino rate induced by vacuum oscillations. The solid curve represents the deviations of the first Fourier coefficient f_1 from its standard value σ (see [33]), plotted as function of m^2 in the most favorable condition (maximal oscillation amplitude, $\sin^2 2\theta = 1$). The largest vertical error bar corresponds to the ± 1 statistical error estimated in Eq. (4) for one year of operation of SuperKamioke. It can be seen that the 1 yr error bars are as large as the range spanned by variations of $f_1 - \sigma$, which are thus practically undetectable at present. However, the error bars after 2 and 4 years of data taking should be reduced enough to allow some sensitivity to the largest predicted variations. Of course, improvements in the energy threshold or in the background rate might reduce the uncertainties more rapidly than the time sequence shown in Fig. 8.

By comparing Figs. 7 and 8, it can be noticed that the deviations of H/E and of f_1 have the same sign (both positive or negative) at equal values of m^2 . Such correlation between energy spectrum deviations and time variations of the signal can be traced to the $L=E$ dependence of the vacuum oscillation probability, as recently emphasized in [34].

In conclusion, the SuperKamioke energy spectrum data constrain rather strongly the vacuum oscillation solutions, allowing only the restricted range $m^2 \sim 6 \times 10^{11} \text{ eV}^2$ (at large mixing). The present experimental sensitivity does not allow detection of semiannual modulations of the neutrino rate due to oscillations. Detection at greater than 1σ level should require at least one more year of operation, unless the uncertainties get reduced further by improving the energy threshold or the background rate, relative to the present levels.

IV. SUMMARY AND CONCLUSIONS

We have performed a thorough analysis of the solar neutrino problem in two scenarios: MSW and vacuum oscillations (between two neutrino families). We have used the most recent available data, including the preliminary results of the SuperKamioke experiment after 306.3 days of operation. Particular attention has been devoted to the treatment of the new, solar-model independent data, namely, the energy spectrum information and the time variations of the signal in SuperKamioke. It has been shown that: 1) the small mixing angle solution is preferred over the large angle one; 2) the vacuum oscillation solutions are strongly constrained by the energy spectrum measurements; and 3) the detection of semiannual modulations of the ^8B neutrino flux in SuperKamioke should require at least one more year of operation.

ACKNOWLEDGMENTS

D.M. thanks the International School for Advanced Studies (SISSA, Trieste, Italy), and in particular A. Masiero and S.T. Petcov, for kind hospitality during the early stages of this work. E.L. thanks K. Inoue and A. Yu. Smirnov for helpful conversations during the TAUP '97 Workshop.

APPENDIX : EVALUATION OF $\langle E_e \rangle$ FROM THE SUPERKAMIOKANDE SPECTRUM

In this Appendix we give the detailed derivation of the result reported in Eq. (1). We make use of the preliminary SuperKamioKANDE spectrum data after 306.3 days of operation [14{16], as reported in Table II and shown in Fig. 4.

The average value of the total electron energy $\langle E_e \rangle$ from the unbinned theoretical spectrum $n(E_e)$ (solid curve in Fig. 4) is given by

$$\langle E_e \rangle_{\text{theo}} (\text{unbinned}) = \frac{\int_{6.5 \text{ MeV}}^{20 \text{ MeV}} dE_e n(E_e) E_e}{\int_{6.5 \text{ MeV}}^{20 \text{ MeV}} dE_e n(E_e)} = 8.536 \text{ MeV} : \quad (\text{A } 1)$$

Using instead the binned theoretical spectrum n_i from Table II one obtains:

$$\langle E_e \rangle_{\text{theo}} (\text{binned}) = \frac{\sum_{i=1}^{16} n_i E_i}{\sum_{i=1}^{16} n_i} = 8.525 \text{ MeV} : \quad (\text{A } 2)$$

The difference between the values in Eqs. (A 1) and (A 2) is only 0.1%, indicating that the effect of binning is not important in the evaluation of the average energy. We will anyway attach to $\langle E_e \rangle_{\text{theo}}$ a "binning error" that, as we shall see, is an order of magnitude smaller than the present experimental uncertainties. Another small error is induced by the ^8B neutrino spectrum uncertainty (as shown by the dotted curves in Fig. 4), that we evaluate as $\langle E_e \rangle_{\text{theo}} = 0.016 \text{ MeV}$ at the 1 level.

The average value of $\langle E_e \rangle$ derived from the (binned) experimental spectrum is given by

$$\langle E_e \rangle_{\text{exp}} = \frac{\sum_{i=1}^{16} n_i r_i E_i}{\sum_{i=1}^{16} n_i r_i} = 8.604 \text{ MeV} ; \quad (\text{A } 3)$$

where r_i and E_i are given in Table II. In general, the squared error $\sigma_{\langle E_e \rangle}^2$ associated to $\langle E_e \rangle_{\text{exp}}$ reads

$$\sigma_{\langle E_e \rangle}^2 = \sum_{i=1}^{16} \sum_{j=1}^{16} \frac{\partial \langle E_e \rangle_{\text{exp}}}{\partial r_i} \frac{\partial \langle E_e \rangle_{\text{exp}}}{\partial r_j} \rho_{ij} ; \quad (\text{A } 4)$$

where ρ_{ij} represents the error of r_i and ρ_{ij} is the correlation matrix. The partial derivatives are easily obtained from Eq. (A 3):

$$\frac{\partial \langle E_e \rangle_{\text{exp}}}{\partial r_i} = n_i \frac{E_i}{\sum_{j=1}^{16} n_j r_j} : \quad (\text{A } 5)$$

The correlation coefficients for the statistical and uncorrelated systematic errors are given by $\rho_{ij} = \delta_{ij}$, so that from Eq. (A 4) one obtains

$$\sigma_{\langle E_e \rangle}^2 (\text{stat.} + \text{uncorr. syst.}) = \sum_{i=1}^{16} \frac{\partial \langle E_e \rangle_{\text{exp}}}{\partial r_i}^2 \frac{1}{r_i^2} = \frac{1}{0.055} + 0.108 \quad (\text{MeV}) ; \quad (\text{A } 6)$$

where the σ_i^0 's are taken from Table II, upper and lower errors being propagated separately. The remaining systematic errors are fully correlated [16], i.e., $\rho_{ij} = 1$, so that

$$hE_i(\text{corr: syst:}) = \sum_{i=1}^{16} \frac{\partial hE_{e,i,\text{exp}}}{\partial r_i} \sigma_i^0 = {}^{+0.170}_{-0.050} \text{ (MeV)} ; \quad (\text{A } 7)$$

where the σ_i^0 's are given in the last two columns of Table II.

Taking the difference between Eqs. (A 3) and (A 2) and including all the uncertainties, one obtains

$$hE_{i,\text{exp}} - hE_{i,\text{theo}} = {}^{+0.108}_{-0.055} {}^{+0.170}_{-0.050} {}^{+0.010}_{-0.016} \text{ (MeV)} ; \quad (\text{A } 8)$$

where the first error is due to statistics and to uncorrelated systematics, the second to correlated systematics, the third to the electron spectrum binning, and the fourth to the ${}^8\text{B}$ neutrino spectrum uncertainties. In conclusion, passing from total to kinetic energies, it follows that

$$\frac{hT_{i,\text{exp}} - hT_{i,\text{theo}}}{hT_{i,\text{theo}}} = {}^{+2.52}_{-0.96} \% ; \quad (\text{A } 9)$$

having added in quadrature the 1 independent errors in Eq. (A 8). This is the final result anticipated in Eq. (1).

TABLES

TABLE I. Neutrino event rates measured by solar neutrino experiments, and corresponding predictions from the BP 95 standard solar model. The quoted errors are at 1 σ .

Experiment	Ref.	Data			Theory [6]	Units
Homestake	[17]	2.54	0.16	0.14	$9.3^{+1.2}_{-1.4}$	SNU
Kamionkande	[8]	2.80	0.19	0.23	$6.62^{+0.93}_{-1.12}$	$10^6 \text{ cm}^{-2} \text{ s}^{-1}$
SAGE	[18]	73	$8.5^{+5.2}_{-6.9}$		137^{+8}_{-7}	SNU
GALLEx	[19]	76.2	6.5	5	137^{+8}_{-7}	SNU
SuperKamionkande	[14]	2.44	$0.06^{+0.25}_{-0.09}$		$6.62^{+0.93}_{-1.12}$	$10^6 \text{ cm}^{-2} \text{ s}^{-1}$

TABLE II. The electron energy spectrum at SuperKamionkande. First three columns: sequential number, energy range, and average energy for each bin. Fourth column: expected number of events n_i per bin per day per kiloton without oscillations (our calculation). Fifth column: ratio of measured to expected rates in each bin. Sixth and seventh columns: Upper and lower 1 σ errors of r_i from statistical and uncorrelated systematic uncertainties. Eighth and ninth columns: Upper and lower 1 σ errors of r_i from correlated systematic uncertainties. The numbers in columns 6{9 have been graphically reduced from the plots shown in [14]{16].

i	Range ^a	E _i ^a	n _i ^b	r _i	⁰ _i (stat.+ unc.)	⁰⁰ _i (corr. syst.)		
1	[6.5; 7]	6.747	0.309	0.346	+ 0.046	0.032	+ 0.010	0.004
2	[7; 7.5]	7.244	0.271	0.341	+ 0.045	0.032	+ 0.013	0.006
3	[7.5; 8]	7.742	0.232	0.350	+ 0.043	0.036	+ 0.016	0.008
4	[8; 8.5]	8.239	0.198	0.400	+ 0.062	0.037	+ 0.025	0.010
5	[8.5; 9]	8.742	0.165	0.327	+ 0.064	0.039	+ 0.026	0.012
6	[9; 9.5]	9.240	0.135	0.373	+ 0.075	0.046	+ 0.040	0.014
7	[9.5; 10]	9.736	0.109	0.382	+ 0.092	0.049	+ 0.050	0.016
8	[10; 10.5]	10.239	0.087	0.373	+ 0.101	0.053	+ 0.058	0.017
9	[10.5; 11]	10.737	0.066	0.356	+ 0.115	0.059	+ 0.069	0.023
10	[11; 11.5]	11.234	0.050	0.372	+ 0.138	0.062	+ 0.089	0.026
11	[11.5; 12]	11.736	0.036	0.392	+ 0.170	0.072	+ 0.110	0.036
12	[12; 12.5]	12.234	0.026	0.402	+ 0.209	0.088	+ 0.137	0.042
13	[12.5; 13]	12.730	0.017	0.359	+ 0.229	0.098	+ 0.141	0.046
14	[13; 13.5]	13.232	0.012	0.422	+ 0.238	0.123	+ 0.192	0.063
15	[13.5; 14]	13.730	0.007	0.627	+ 0.506	0.183	+ 0.337	0.101
16	[14; 20]	14.817	0.010	0.493	+ 0.510	0.170	+ 0.378	0.114

^aUnits: MeV (total electron energy).

^bUnits: events/day/kton/bin.

TABLE III. Number of signal events N_S and signal-to-background ratio N_S/N_B for various \cos_{sun} thresholds (as derived from the \cos_{sun} event spectrum presented in [14{16}], together with the corresponding uncertainty δ_f of the deviation of the first Fourier coefficient f_1 from its standard value " [see Eq. (3)].

\cos_{sun}	N_S	N_S/N_B	δ_f
> 0.5	4100	0.30	0.023
> 0.6	3870	0.35	0.022
> 0.7	3620	0.38	0.021
> 0.8	3270	0.59	0.020
> 0.9	2530	0.92	0.020

REFERENCES

- [1] J.N. Bahcall, *Neutrino Astrophysics* (Cambridge University Press, Cambridge, England, 1989).
- [2] R. Davis (Homestake Collaboration), *Prog. Part. Nucl. Phys.* 32, 13 (1994).
- [3] K. S. Hirata et al. (Kamiokande Collaboration), *Phys. Rev. Lett.* 65, 1297 (1990); 65, 1301 (1990); 66, 9 (1991); *Phys. Rev. D* 44, 2241 (1991); 45, 2170 (E) (1992).
- [4] J.N. Abdurashitov et al. (SAGE Collaboration), *Phys. Lett. B* 328, 234 (1994); *Phys. Rev. Lett.* 77, 4708 (1996).
- [5] P. Anselmann et al. (GALLEx Collaboration), *Phys. Lett. B* 327, 377 (1994); 357, 237 (1995); 361, 235 (E) (1996); W. Hampel et al., 288, 384 (1996).
- [6] J.N. Bahcall and M. H. P.insonneault, *Rev. Mod. Phys.* 67, 781 (1995).
- [7] B. Cleveland et al. (Homestake Collaboration), in *Neutrino '94, Proceedings of the 16th International Conference on Neutrino Physics and Astrophysics*, Eilat, Israel, 1994, edited by A. Dar, G. Eilam, and M. Gronau, *Nucl. Phys. B (Proc. Suppl.)* 38, 47 (1995).
- [8] Y. Fukuda et al. (Kamiokande Collaboration), *Phys. Rev. Lett.* 77, 1683 (1996).
- [9] V. N. Gavrin et al. (SAGE Collaboration), in the *Proceedings of the 7th International Workshop on Neutrino Telescopes*, Venice, Italy, 1996, edited by M. Baldo Ceolin (University of Padua, Italy, 1996), p. 205.
- [10] P. Anselmann et al. (GALLEx Collaboration), *Phys. Lett. B* 342, 440 (1995); M. Cribier et al., *Nucl. Instr. and Methods A* 378, 233 (1996).
- [11] J.N. Bahcall, M. H. P.insonneault, S. Basu, and J. Christensen-Dalsgaard, *Phys. Rev. Lett.* 78, 171 (1997).
- [12] B. Ricci, V. Berezinsky, S. D'egl'Innocenti, W. A. Dziembowski, and G. Fiorentini, *Phys. Lett. B* 407, 155 (1997).
- [13] A. Suzuki, in *Physics and Astrophysics of Neutrinos*, edited by M. Fukugita and A. Suzuki (Springer-Verlag, Tokyo, 1994), p. 414; Y. Totsuka, *ibidem*, p. 625.
- [14] Y. Totsuka (SuperKamiokande Collaboration), in *LP '97, 28th International Symposium on Lepton Photon Interactions*, Hamburg, Germany, 1997, to appear in the *Proceedings*.
- [15] M. Nakahata (SuperKamiokande Collaboration), in *HEP '97, International Europhysics Conference in High Energy Physics*, Jerusalem, Israel, 1997, to appear in the *Proceedings*.
- [16] K. Inoue (SuperKamiokande Collaboration), in *TAUP '97 5th International Workshop on Topics in Astroparticle and Underground Physics*, Laboratori Nazionali del Gran Sasso, Assergi, Italy, 1997, to appear in the *Proceedings*.
- [17] K. Lande (Homestake Collaboration), in the *4th International Solar Neutrino Conference*, Heidelberg, Germany, 1997, to appear in the *Proceedings*.
- [18] SAGE Collaboration, as reported in [14].
- [19] M. Cribier (GALLEx Collaboration), in *TAUP '97* [16].
- [20] V. N. Gribov and B. M. Pontecorvo, *Phys. Lett. B* 28, 493 (1969); J.N. Bahcall and S. C. Frautschi, *Phys. Lett. B* 29, 623 (1969); S. L. Glashow and L. M. Krauss, *Phys. Lett. B* 190, 199 (1987).
- [21] L. Wolfenstein, *Phys. Rev. D* 17, 2369 (1978); S. P. Mikheyev and A. Yu. Smirnov, *Yad. Fiz.* 42, 1441 (1985) [*Sov. J. Nucl. Phys.* 42, 913 (1986)]; *Nuovo Cimento C* 9, 17 (1986).

- [22] G . L . Fogli and E . Lisi, *Astropart. Phys.* 3, 185 (1995).
- [23] G . L . Fogli, E . Lisi, and D . M ontanino, *Phys. Rev. D* 49, 3426 (1994); *Astropart. Phys.* 4, 177 (1995).
- [24] G . L . Fogli, E . Lisi, and D . M ontanino, *Phys. Rev. D* 54, 2048 (1996).
- [25] N . Hata and P . Langacker, University of Pennsylvania Report No. UPR -0751-T, hep-ph/9705339, to appear in *Phys. Rev. D*.
- [26] P . I . K rastev and S . T . Petrov, *Phys. Lett. B* 285, 85 (1992); *Phys. Rev. D* 53, 1665 (1996).
- [27] J . N . Bahcall, E . Lisi, D . E . Alburger, L . De Braeckeleer, S . J . Freedman, and J . Napolitano, *Phys. Rev. C* 54, 411 (1996).
- [28] J . N . Bahcall, M . Kam ionkowsky, and A . Sirlin, *Phys. Rev. D* 51, 6146 (1995).
- [29] E . Lisi and D . M ontanino, *Phys. Rev. D* 56, 1792 (1997).
- [30] B . Fa d, G . L . Fogli, E . Lisi, and D . M ontanino, *Phys. Rev. D* 55, 1353 (1997).
- [31] J . N . Bahcall and E . Lisi, *Phys. Rev. D* 54, 5417, (1996).
- [32] J . N . Bahcall, P . I . K rastev, and E . Lisi, *Phys. Rev. C* 55, 494 (1997).
- [33] G . L . Fogli, E . Lisi, and D . M ontanino, *Phys. Rev. D* 56, 4374 (1997).
- [34] S . P . M ikheyev and A . Yu . Sm imov, International Centre for Theoretical Physics (ICTP, Trieste) Report No. IC -97-113, hep-ph/9708403.

FIGURES

FIG .1. The current state of the solar neutrino deficit. The ellipses represent the regions allowed at 99% C.L. by the present solar neutrino data (dashed lines) and by the standard solar model (SSM) of Bahcall-Pinsonneault [6]. The coordinates are the chlorine (Cl), gallium (Ga), and water-Cherenkov [normalized (K + SuperK)/SSM] neutrino rates.

FIG .2. The MSW small and large mixing angle solutions to the solar neutrino problem, as obtained by a fit to the total rates only (energy spectrum and night-day data not included).

FIG .3. The vacuum oscillation solutions to the solar neutrino problem, as obtained by a fit to the total rates only (energy spectrum and night-day data not included). The range of the (logarithmic) vertical scale is $(0.5\{2\} \times 10^{-10} \text{ eV}^2)$.

FIG .4. The electron recoil energy spectrum at SuperKamiokande. The dots represent the measured rates in each energy bin, with vertical 1 σ error bars given by the quadratic sum of statistical and systematic errors. The horizontal bars span the bin widths. Also shown is the standard spectrum expected in the absence of oscillations (solid line), together with the spectra obtained by assuming ± 3 deviations of the standard ^8B neutrino spectrum [27]. The data are taken from [14][16]. The theoretical spectra refer to our calculations, renormalized to give the same area as the experimental histogram.

FIG .5. Constraints on the MSW solutions as derived by the measured value of the average electron kinetic energy $\langle T_i \rangle$. Upper panel: Theoretical expectations for the fractional shift of $\langle T_i \rangle$ from its standard (no oscillation) value $\langle T_{i0} \rangle$. Lower panel: regions excluded at 2, 3, and 4 standard deviations by the SuperKamiokande determination of $\langle T_i \rangle$.

FIG .6. Constraints on the MSW solutions as derived by the measured value of the asymmetry of nighttime (R_N) and daytime (R_D) event rates. Upper panel: theoretical expectations for $(R_N - R_D)/(R_N + R_D)$. Lower panel: Regions excluded at 2, 3, and 4 standard deviations by the SuperKamiokande data.

FIG .7. Constraints on the vacuum oscillation solutions as derived by the measured value of the average electron kinetic energy $\langle T_i \rangle$. Upper panel: Theoretical expectations for the fractional shift of $\langle T_i \rangle$ from its standard (no oscillation) value $\langle T_{i0} \rangle$. Lower panel: Regions excluded at 2, 3, and 4 standard deviations by the SuperKamiokande determination of $\langle T_i \rangle$.

FIG .8. Fourier analysis of time variations induced by vacuum oscillations. Solid curve: expected deviations of the first Fourier coefficient f_1 from its standard value (equal to Earth orbital eccentricity e) for $\sin^2 2\theta = 1$. Error bars: Our estimate of the statistical errors of SuperKamiokande (including background) after 1, 2, and 4 years of data taking. See the text and [33] for details.

Solar neutrino deficit, 1997

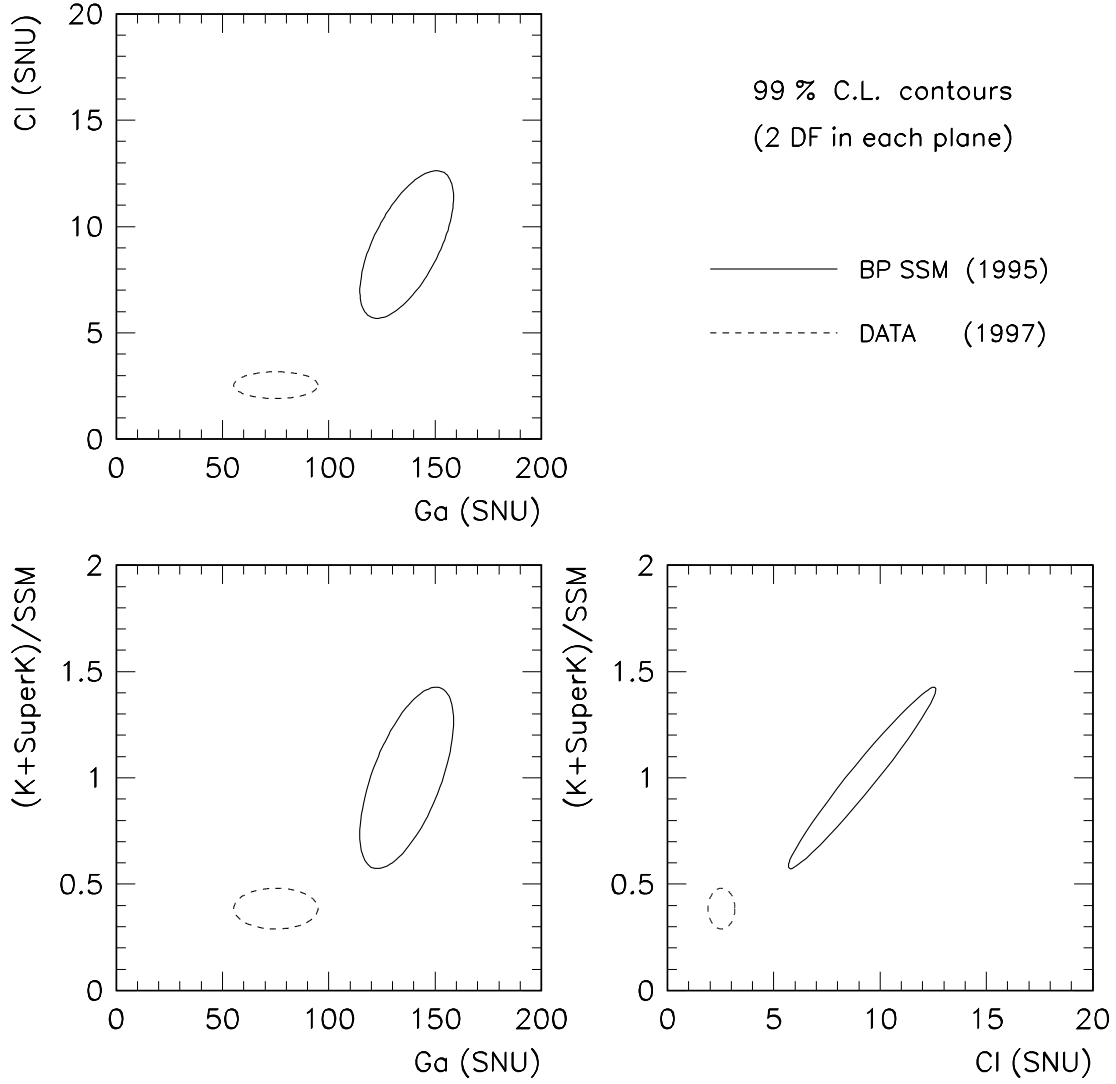


FIG. 1. The current state of the solar neutrino deficit. The ellipses represent the regions allowed at 99% C.L. by the present solar neutrino data (dashed lines) and by the standard solar model (SSM) of Bahcall-Pinsonneault [6]. The coordinates are the chlorine (Cl), gallium (Ga), and water-Cherenkov [normalized (K + SuperK)/SSM] neutrino rates.

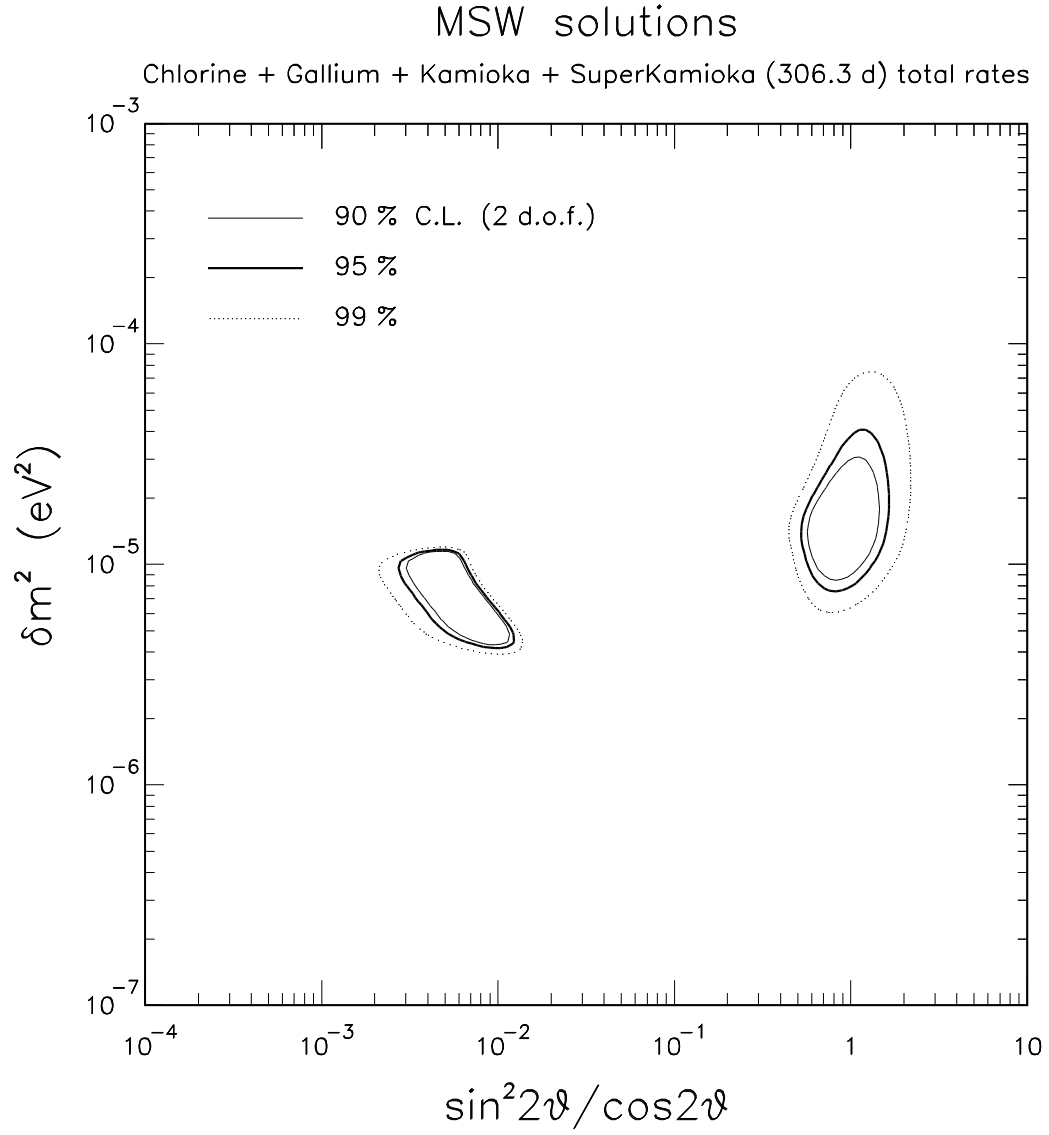


FIG. 2. The MSW small and large mixing angle solutions to the solar neutrino problem, as obtained by a fit to the total rates only (energy spectrum and night-day data not included).

Vacuum solutions

Chlorine + Gallium + Kamioka + SuperKamioka (306.3 d) total rates

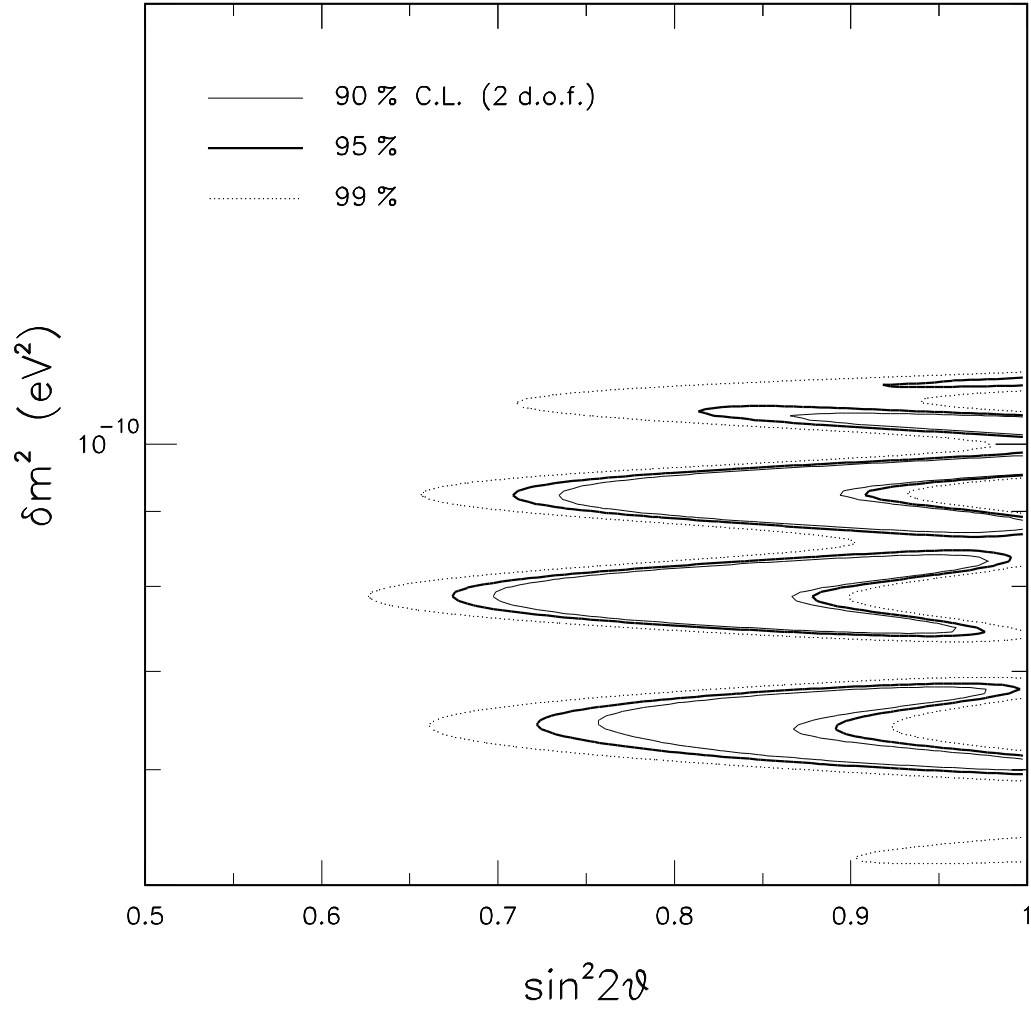


FIG. 3. The vacuum oscillation solutions to the solar neutrino problem, as obtained by a fit to the total rates only (energy spectrum and night-day data not included). The range of the (logarithmic) vertical scale is $(0.5\{2\}) \cdot 10^{-10} \text{ eV}^2$.

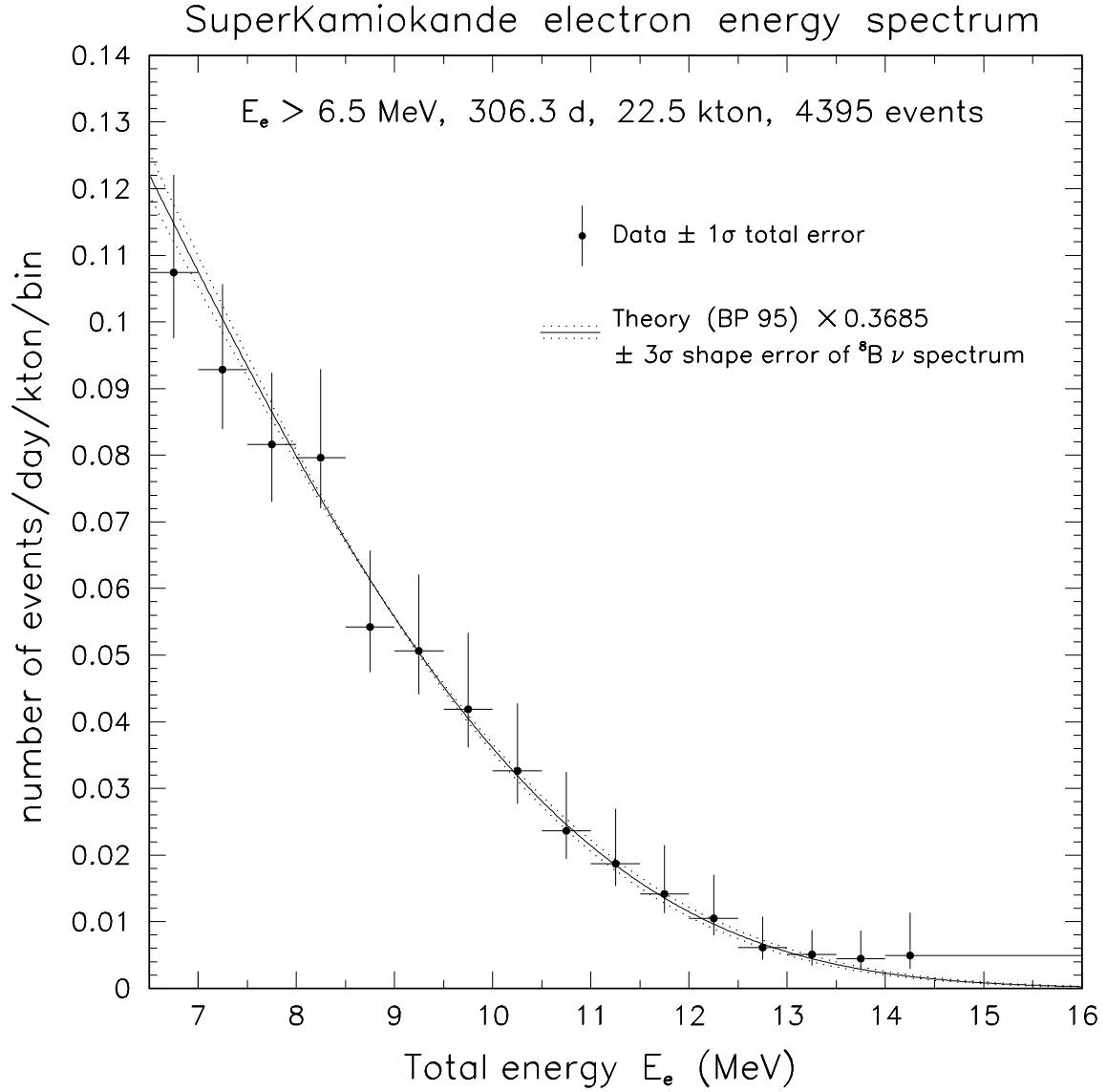


FIG . 4. The electron recoil energy spectrum at SuperKam iokande. The dots represent the measured rates in each energy bin, with vertical 1σ error bars given by the quadratic sum of statistical and systematic errors. The horizontal bars span the bin widths. Also shown is the standard spectrum expected in the absence of oscillations (solid line), together with the spectra obtained by assuming ± 3 deviations of the standard ^8B neutrino spectrum [27]. The data are taken from [14][16]. The theoretical spectra refer to our calculations, renormalized to give the same area as the experimental histogram.

SuperKamiokande, energy spectrum

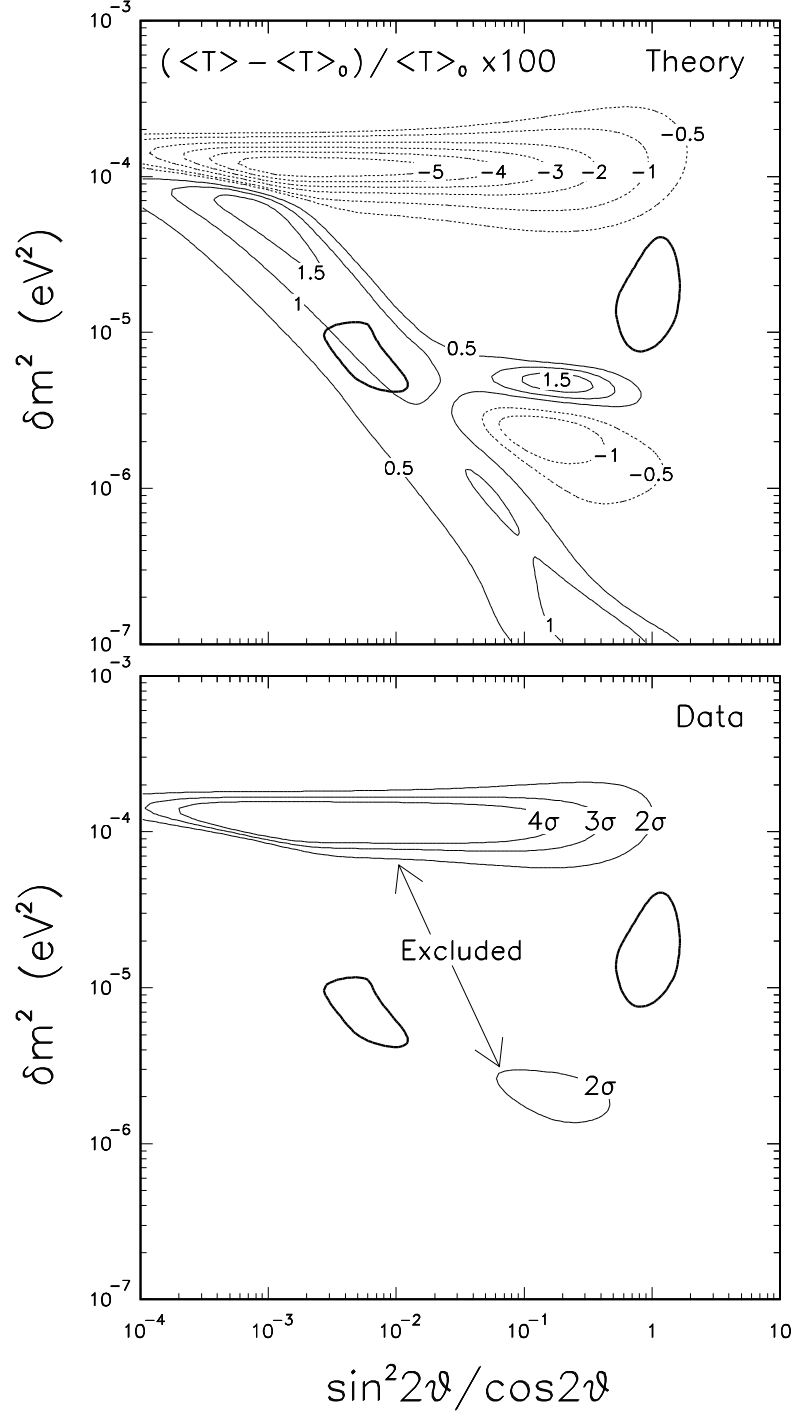


FIG. 5. Constraints on the M SW solutions as derived by the measured value of the average electron kinetic energy $\langle T \rangle$. Upper panel: Theoretical expectations for the fractional shift of $\langle T \rangle$ from its standard (no oscillation) value $\langle T \rangle_0$. Lower panel: regions excluded at 2, 3, and 4 standard deviations by the SuperKamioKande determination of $\langle T \rangle$.

SuperKamiokande, Night–Day asymmetry

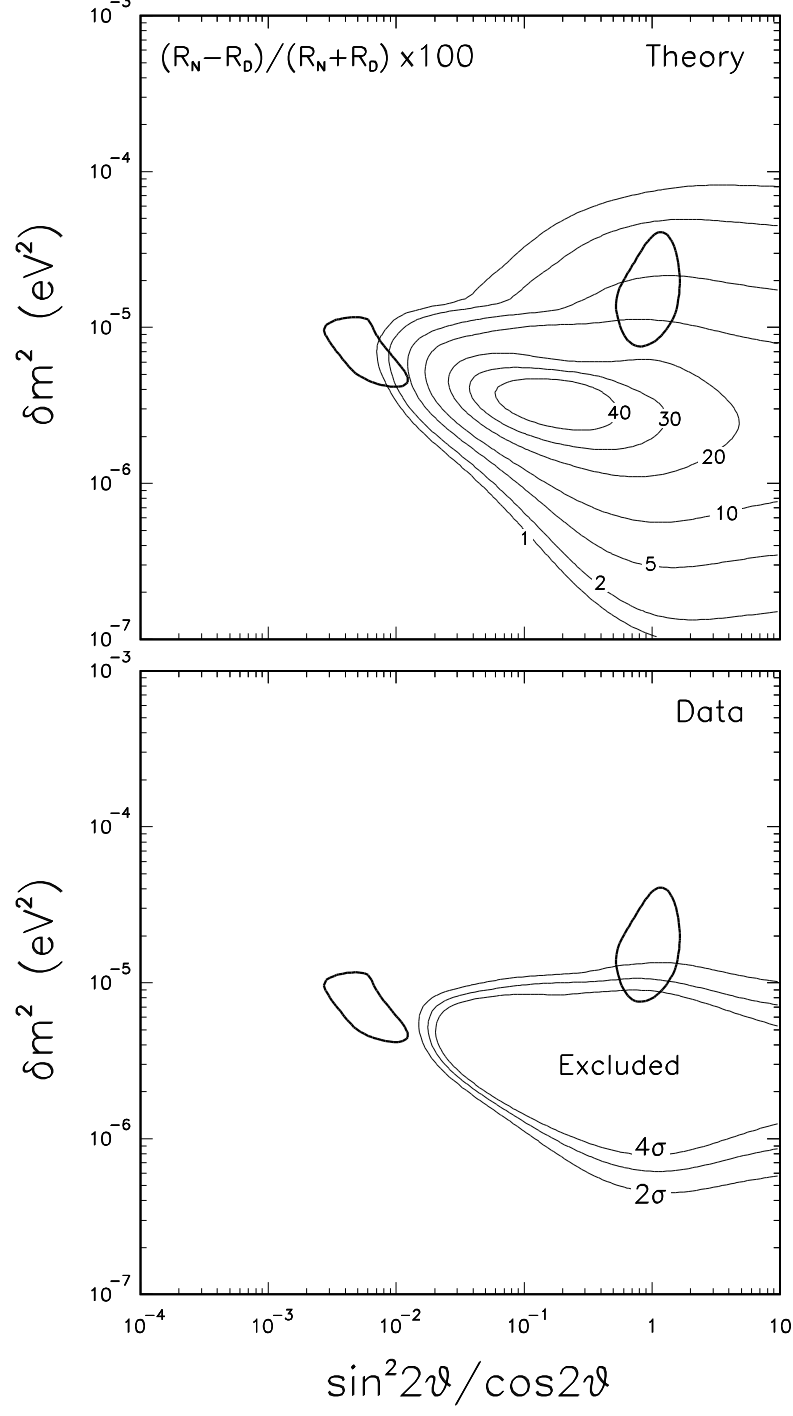


FIG. 6. Constraints on the MSW solutions as derived by the measured value of the asymmetry of nighttime (R_N) and daytime (R_D) event rates. Upper panel: theoretical expectations for $(R_N - R_D)/(R_N + R_D)$. Lower panel: Regions excluded at 2, 3, and 4 standard deviations by the SuperKamiokande data.

SuperKamiokande, energy spectrum

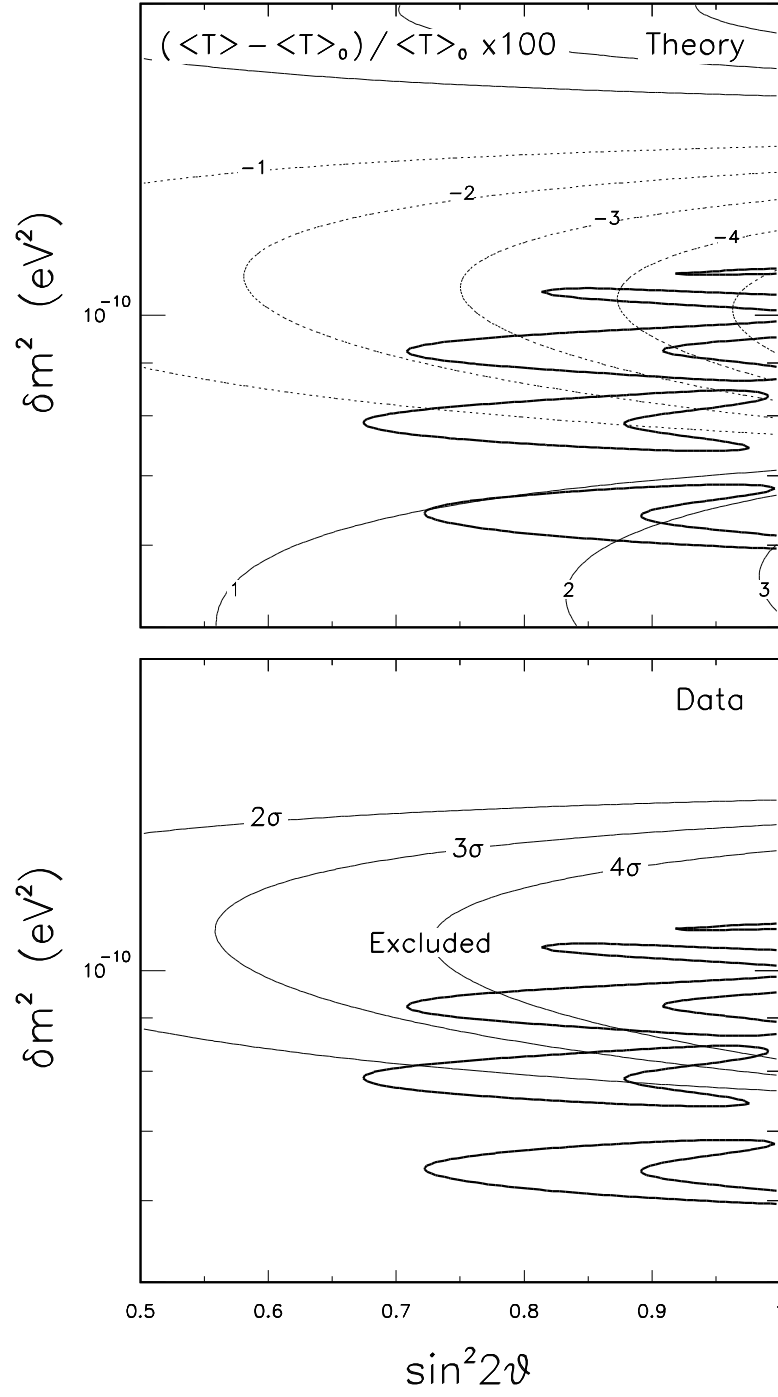


FIG . 7. Constraints on the vacuum oscillation solutions as derived by the measured value of the average electron kinetic energy $\langle T \rangle$. Upper panel: Theoretical expectations for the fractional shift of $\langle T \rangle$ from its standard (no oscillation) value $\langle T \rangle_0$. Lower panel: Regions excluded at 2, 3, and 4 standard deviations by the SuperKamioke determination of $\langle T \rangle$.

SuperKamiokande, vacuum oscillations

Deviation of first Fourier coefficient from standard value

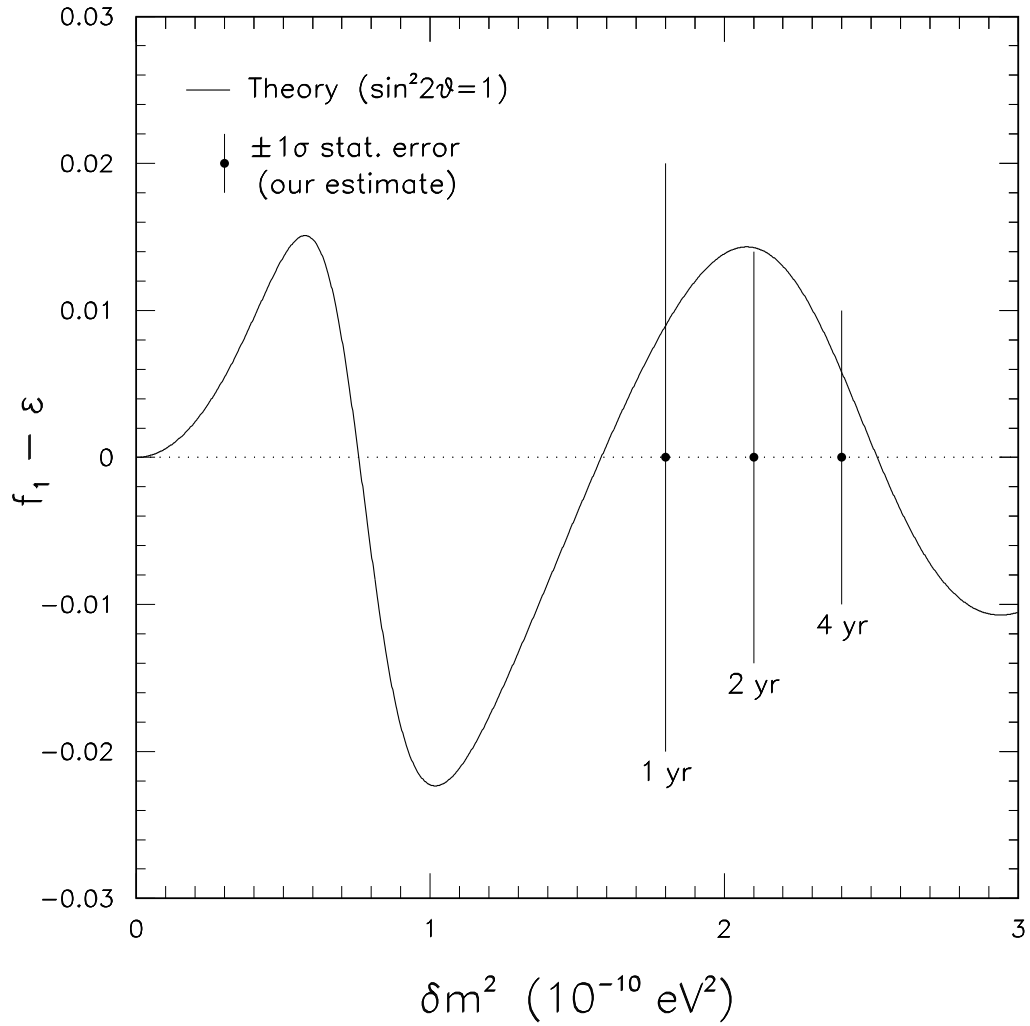


FIG .8. Fourier analysis of the variations induced by vacuum oscillations. Solid curve: expected deviations of the first Fourier coefficient f_1 from its standard value (equal to Earth orbit eccentricity) for $\sin^2 2\theta = 1$. Error bars: Our estimate of the statistical errors of SuperKamiokande (including background) after 1, 2, and 4 years of data taking. See the text and [33] for details.